Variations in vegetation evapotranspiration affect water yield in high-altitude areas

Yinying Jiao[1,2,3], Guofeng Zhu[1,2,3*], Dongdong Qiu[1,2,3], Siyu Lu[1,2,3], Gaojia Meng[1,2,3], Rui Li[1,2,3],Qinqin Wang[1,2,3], Longhu Chen[1,2,3], Wentong Li[1,2,3]

5 [1]College of Geography and Environment Science, Northwest Normal University, Lanzhou 730070, Gansu, China
[2]Shiyang River Ecological Environment Observation Station, Northwest Normal University, Lanzhou 730070, Gansu, China
[3]Key Laboratory of Resource Environment and Sustainable Development of Oasis, Gansu Province, Lanzhou 730070, Gansu, China

Correspondence to: Guofeng Zhu (zhugf@nwnu.edu.cn)

10 **Abstract.** Global mountains and plateaus are the main water-producing areas on land. However, under the influence of climate change, the distribution of vegetation and the way water is utilized in these areas have undergone significant changes. As such, understanding the effects of evapotranspiration from high-altitude vegetation on precipitation and runoff is vital in addressing the uncertainties and challenges posed by climate change and anthropogenic transformation. The stable isotopes in water bodies play a crucial role in determining the evapotranspiration capacity of ecosystems and the mechanisms of
15 precipitation formation. Between 2018 and 2022, we conducted research in the northeastern Qinghai-Tibet Plateau, collected and analyzed stable isotope water data from precipitation, soil water, and Picea crassifolia xylem water to quantify the impact of vegetation transpiration and recirculated water vapor on precipitation. Our findings indicate that transpiration from vegetation accounts for the largest share of evapotranspiration within the entire forest ecosystem, averaging 57%. Therefore, vegetation transpiration is the decisive factor in determining the water yield of inland high-altitude areas. Local
20 evapotranspiration contributes an average of 28% to precipitation, further enhancing the replenishment of precipitation in high-altitude areas. The warming of global temperatures and human activities are likely to induce shifts in the distribution areas and evapotranspiration regimes of alpine vegetation, potentially altering water resource patterns in the basin. It is necessary to actively adapt to the changes in water resources in the inland river basin.

1 Introduction

25 Projected future scenarios suggest that drought events will become more frequent, severe, and prolonged due to the effects of climate change. This phenomenon is expected to manifest most rapidly and intensely in arid and semi-arid regions (Ault et al., 2020). Large-scale forest ecosystems play a pivotal role in influencing climate through biophysical feedback mechanisms and in altering the global water cycle. The stable hydrogen and oxygen isotopes found in precipitation, plant water, and soil water can effectively trace evaporation within water cycle. During water evaporation, isotopic fractionation occurs as
30 molecules of differing mass redistribute between the vapor and liquid phases, leaving heavier isotopes such as D and $\delta^{18}O$

predominantly in the liquid phase(Dansgaard et al., 1964). Plant transpiration further enriches heavy isotopes in leaf water, while the heavier and lighter molecules released through stomata remain in equilibrium with the xylem water supply. This mechanism underpins the use of stable isotopes to estimate vegetation transpiration capacity (Farquhar et al., 2007). The Picea crassifolia ecosystem, providing a range of ecological, climatic, and social benefits to the northeastern Tibetan Plateau,

35 exhibits high susceptibility to drought and temperature extremes. Furthermore, climate-related drivers significantly heighten the vulnerability of Picea crassifolia to drought and heat stress, with an anticipated increase in disturbances to its ecosystem as climate change progresses.

Variations in evaporation loss are known to precipitate disturbances in the precipitation and surface water budget (Li et al., 2023). Furthermore, forest evapotranspiration (ET) significantly influences atmospheric moisture convergence and

40 precipitation dynamics, with its impact critically dependent on ambient moisture conditions (Makarieva et al., 2023). Additionally, across different spatial scales, vegetation transpiration capacity and local water availability demonstrate complex and variable relationships. This is specifically reflected in the following aspects. Enhanced evapotranspiration can contribute up to 45% of available water in both local and downwind regions, though this proportion may substantially vary in water-scarce environments (Cui et al., 2022). As precipitation recycling and moisture convergence intensify, the

45 sensitivity of precipitation to evapotranspiration becomes increasingly pronounced (Cheng et al., 2024). In regions characterized by high vegetation cover and elevated topography, moisture recycling significantly enhances regional water resource availability (An et al., 2025). The upward movement of water vapor in the atmosphere, upon merging with advection water vapor, condenses to form precipitation. Consequently, in high-altitude areas with greater vegetation coverage and favorable conditions for moisture convergence, precipitation is typically more abundant. The trajectory and

50 intensity of westerly winds critically determine moisture content and precipitation distribution across Central Asian mountain ranges, particularly during the cold season under the substantial influence of the subtropical westerly jet (Mehmood et al., 2022). Even minor redistributions of atmospheric water can trigger significant cascading effects, inducing substantial shifts in latent heat flux, atmospheric circulation, water transport mechanisms, and precipitation patterns (Hao et al., 2023). Moreover, for high-altitude regions influenced by the cryosphere, the mechanism by which vegetation-dominated

55 water vapor contributes to precipitation and runoff formation remains a critical knowledge gap.

As a vascular plant species, Picea crassifolia plays a crucial role in channeling energy and materials from the environment into terrestrial ecosystems. Its growth, survival, and reproduction significantly influence the ecological functions and structures of other species, both within their habitats and in broader ecological contexts. A significant interaction exists between the vegetation, its drought resilience, and the microclimatic conditions within forests and their ecosystems. This

60 interaction is vital for understanding ecosystem dynamics (Eisenhauer et al., 2021). In this study, we conducted monthly observations and analyses of the xylem water potential, soil water potential, stable isotopes of precipitation, and soil water content of Picea crassifolia in the northeastern Qinghai-Tibet Plateau from April to October for the years 2018 and 2022. These data were utilized to address the following research objectives: (1) To quantify the contribution rates of soil evaporation and vegetation transpiration to the total evapotranspiration of ecosystems; (2) To determine the ratio of

65 recirculated water vapor in precipitation; and (3) To investigate the evapotranspiration process and its impact on productivity and hydrological convergence in the forest belt of the mountainous region. This study provides a robust foundation for the management of local water resources and the protection of ecological integrity.

2 Study area

The Qilian Mountains are located in the central part of the Eurasian continent, on the northeastern edge of the Qinghai-Tibet
70 Plateau(Figure 1). The eastern region is dominated by water erosion, with large variations in mountainous terrain and an average elevation of over 4,000 meters. Permafrost is developed at elevations of 3,500 to 3,700 meters, and areas above 4,500 meters are characterized by modern glacier development. The region has a plateau continental climate, with hot summers and cold winters, strong solar radiation, and large temperature differences between day and night. The average annual temperature is below 4℃, with extreme highs of 37.6℃ and extreme lows of -35.8℃. The annual sunshine hours
75 range from 2,500 to 3,300 hours, with a total solar radiation of 5,916 to 15,000 megajoules per square meter. The average annual precipitation is 400 millimeters, and the annual evaporation ranges from 1,137 to 2,581 millimeters. The average wind speed is around 2 meters per second, and the frost-free period lasts from 23.6 to 193 days. The Shiyang River originates from the Daxueshan on the northern side of the Lenglong Ridge in the eastern section of the Qilian Mountains, serving as a major water source for the city of Wuwei. The soil types in the eastern section are diverse, but with low organic
80 matter content. The distribution of vegetation shows distinct zonal characteristics, with mountainous forest-grassland zones (2,600 to 3,400 meters), subalpine shrub-meadow zones (3,200 to 3,500 meters), and high mountain sub-ice-snow sparse vegetation zones (>3,500 meters) at elevations above 2,700 meters. The main types of natural forest vegetation include Picea crassifolia, Qilian juniper forest, and Chinese pine forest, with Picea crassifolia being the dominant tree species (Zhu et al., 2022).

85
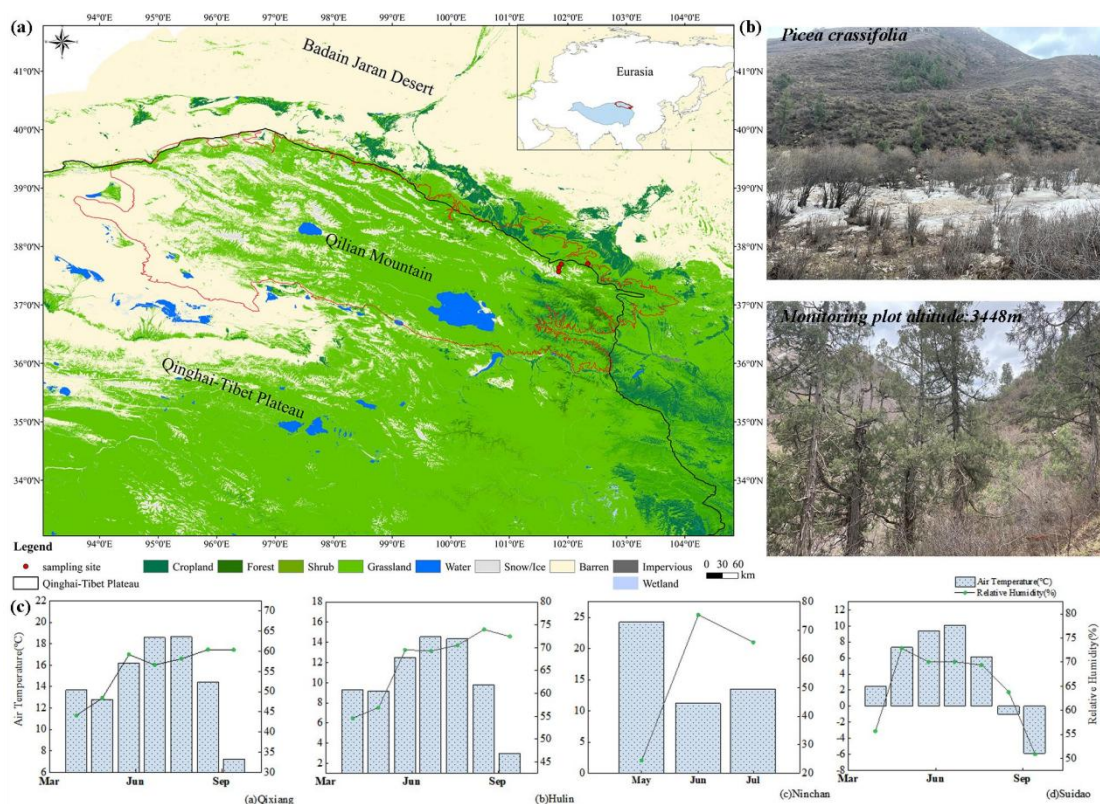
Figure 1: Overview of the study area. (a) Geographical location of the study area, (b) Growth status of Qinghai spruce, and (c) Seasonal variation of meteorological conditions.

3 Materials and methods

3.1 Materials Sources

90   In this study, we established a stable isotope observation network at four elevation zones (2543m, 2721m, 3068m, 3448m) in terms of vertical height (Table 1). Meteorological data were recorded using an automatic weather station in the years 2018 and 2022. The collected precipitation was subsequently transferred to 100ml containers following each rainfall event. Soil samples were extracted from the sample plot at various depths, specifically at intervals of 0-5 cm, 5-10 cm, 10-20 cm, 20-30 cm, 30-40 cm, 40-50 cm, 50-60 cm, 60-70 cm, 70-80 cm, 80-90 cm, and 90-100 cm, utilizing a soil drill. These samples

95   were bifurcated, with one portion being stored in a 50 ml glass bottle. This bottle was hermetically sealed with a parafilm and transported to the observation station, where it was marked with the sampling date and subjected to cryopreservation within 10 hours for the purpose of stable isotope analysis. The remaining portion of the soil sample was placed in a 50ml aluminum box to ascertain soil moisture content through a drying method. For the collection of plant samples, scissors were

4

employed to harvest the xylem stems of vegetation. The bark was removed, and the samples were placed in 50ml glass bottles, which were then sealed and frozen for subsequent experimental analysis.

Table 1:Sampling location, the meteorological background, and sampling quantity information during the growing season.

Parameter	Station	Qixiang	Hulin	Ninchan	Suidao
	Altitude(m)	2543	2721	3068	3448
Local climate	Temperature(°C)	3	3.2	3.3	-0.9
	Precipitation(mm)	262	370	394	475
	Relative humidity（%）	52.9	56.1	66.6	69.2
Samplin gs number	Precipitation	53	108	91	135
	Soil water	220	560	560	560
	Xylem water	236	56	56	56

Surface evapotranspiration data at an elevation of 2700 m were sourced from the MODIS-based daily surface evapotranspiration dataset for the Qilian Mountains. Evapotranspiration data at 3200 m were obtained from high-quality literature that includes field-observed ET values within the elevation range of 2500 to 3400 m to reinforce our research findings. Precipitation data at different elevations were all sourced from the National Tibetan Plateau Data Center.

3.2 Experimental Analysis

The isotopic data used in this study mainly include stable isotopes of precipitation, soil water, and xylem water. All isotopic samples were analyzed at the Stable Isotope Laboratory of Northwest Normal University. The precipitation samples were analyzed for hydrogen and oxygen stable isotopes using a liquid water isotope analyzer (DLT-100, Los Gatos Research, USA). After thawing the soil and vegetation samples, they were extracted using a low-temperature vacuum condensation device (LI-2100, LICA United Technology Limited, China), and the extracted water was subjected to isotopic analysis. Each water sample was tested six times to ensure accuracy, with the first two tests considered as interference and only the results of the subsequent four tests were averaged (Zhu et al., 2022). The isotopic measurements are represented by δ, which represents the deviation in parts per thousand of the ratio of two stable isotopes in the sample relative to the ratio in a standard sample. The International Atomic Energy Agency (IAEA) defined the Vienna Standard Mean Ocean Water (VSMOW) in 1968 as the standard for isotopic composition, which is derived from distilled seawater and has a similar isotopic composition to Standard Mean Ocean Water (SMOW).

$$\delta = (\frac{\delta_{Sampling}}{\delta_{Standard}} - 1) \times 1000‰ , \tag{1}$$

3.3 Research methods

First, determining the isotopic composition of water vapor formed from precipitation, vegetation, and soil evaporation serves as the foundation for applying different models. Based on the isotopic values of different water vapor sources, the contribution of vegetation's evapotranspiration to the overall ecosystem evaporation can be established, which is a step in identifying the key factors affecting precipitation. Next, an end-member mixing model is used to quantify the contribution ratio of recycled water vapor in precipitation. The results of this analysis will be used to assess the impact of these key factors on the formation of precipitation. The parameters involved in the methods are all listed in Table S1 of the supporting information.

3.3.1 Isotopic composition of atmospheric water vapour

The stable isotope composition of moisture in ambient air (δ_a) is calculated as follows(Gibson and Reid, 2014;Skrzypek et al., 2015):

$$\delta_a = \frac{\delta_{rain} - k\varepsilon^+}{1 + k\alpha^+ \times 10^{-3}}, \tag{2}$$

where k=1, or by fitting k to some fraction of 1 as the best fit to the local evaporation line,ε^+ is the isotopic fractionation factor. Defined by $\varepsilon^+ = (\alpha^+ - 1) \times 1000$. α^+ about ^2H and ^{18}O are calculated as follows(Horita and Wesolowski, 1994):

$$10^3 \ln^2\alpha^+ = 1158.8T^3/10^9 - 1620.1T^2/10^6 + 794.84T/10^3 - 161.04 + 2.9992 \times 10^9/T^3, \tag{3}$$

$$10^3 \ln^{18}\alpha^+ = -7.685 + 6.7123 \times 10^3/T - 1.6664 \times 10^6/T^2 + 0.35041 \times 10^9/T^3, \tag{4}$$

Here, α^+ is the equilibrium fractionation factor dependent on temperature, and T is the temperature (K). The value of α^+ is usually around 1.01, and the value of ε^+ is typically around 10.

3.3.2 Isotopic composition of soil evaporation

The Craig-Gordon model was used to calculate the stable isotopic composition of soil evaporation water vapour, δ_E, using the following equation(Yepez et al., 2005).

$$\delta_E = \frac{\alpha_e^{-1}\delta_s - h \quad \delta_a - \varepsilon_{eq} - (1-h)\varepsilon_k}{(1-h) + 10^{-3}(1-h)\varepsilon_k}, \tag{5}$$

where $\alpha_e(>1)$ is the equilibrium factor calculated as a function of water surface temperature, δ_S is the stable isotopic composition of liquid water at the evaporating surface of the soil (0 ~ 10 cm average stable isotopic composition of soil water), δ_a is the stable isotopic composition of atmospheric water vapour near the surface, ε_{eq} represents the equilibrium fractionation corresponding to $\varepsilon_{eq} = (1-1/\alpha_e) \times 1000$, ε_k is the kinetic fractionation factor of oxygen is approximately 18.9‰

and h is the atmospheric relative humidity(Gibson and Reid, 2010). For $\delta^{18}O$, α_e is calculated as follows(Raz-Yaseef et al., 2010):

$$\alpha_e = \frac{1.137\times10^6/T^2 - 0.4156\times10^3/T - 2.0667}{1000} + 1 \,, \tag{6}$$

Where T is the soil Kelvin temperature (K) at a depth of 5 cm.

3.3.3 Isotopic composition of plant transpiration

When transpiration is strong, leaf water is in "isotopic stable state", that is, the isotopic composition of leaf transpiration water is equivalent to that of water absorbed by the roots of rain plants at noon. Therefore, the stable isotopic composition of water in plant xylem can be used to represent the stable isotopic composition of water vapor in plant transpiration. The expression is as follows(Aron et al., 2020):

$$\delta_T = \delta_X \,, \tag{7}$$

where δ_X is the isotopic ratio of xylem water and δ_T is the isotopic ratio of transpiration.

3.3.4 Evapotranspiration isotope assessment

The Keeling Plot model describes the linear relationship between the oxygen isotope composition of atmospheric water vapour and its reciprocal concentration . The intercept of the curve on the Y-axis represents the oxygen isotopic composition of evapotranspiration (δ_{ET}) and is expressed as(Keeling, 1958;Wang et al., 2015)：

$$\delta_a = \frac{C_b(\delta_b - \delta_{ET})}{C_a} + \delta_{ET} \,, \tag{8}$$

Where δ_a and C_a represent the atmospheric water vapour oxygen isotopic composition (‰) and water vapour concentration in the ecosystem boundary layer, δ_b and C_b represent the background atmospheric water vapour oxygen isotopic composition and background atmospheric water vapour concentration, and δ_{ET} is the ecosystem evapotranspiration oxygen isotopic composition.

3.3.5 Proportion of vegetation transpiration

The determination of evapotranspiration by means of biotic and abiotic isotopic composition can be used to improve the understanding of community structure and ecosystem function in Picea crassifolia in the northeastern of Tibetan Plateau. Based on the isotope mass balance approach to consider the distribution of major and minor isotopes, the partitioning of evapotranspiration can be achieved using two end-member mixing models (E and T) with the following expression(Kool et al.,2014;Wei et al., 2018):

$$\frac{T}{ET} = \frac{\delta_{ET} - \delta_E}{\delta_T - \delta_E} \,, \tag{9}$$

where δ_{ET}, δ_E and δ_T are the isotopic compositions of evapotranspiration (ET), soil evapotranspiration (E) and plant evapotranspiration (T), respectively, and the isotopic values of the three can be obtained by both direct observation and model estimation.

3.3.6 Bayesian mixing model

Assuming that precipitation vapor is a mixture of advective water vapour and recirculating water vapour, it is understood that the proportion of both precipitation and precipitation water vapour has the same nature. The proportion of precipitation occupied by recycled vapour is calculated as follow(Kong et al., 2013; Wang et al., 2022):

$$f_{re} = \frac{P_{tr}+P_{ev}}{P_{tr}+P_{ev}+P_{adv}} = f_{tr} + f_{ev} , \tag{10}$$

Where P_{tr}, P_{ev} and P_{adv} are precipitation produced by transpiration, surface evaporation and advection, respectively. The relationships among these three types of water vapor and precipitation are as follows (Brubaker et al., 1993; Sang et al., 2023):

$$\delta_{pv} = \delta_{tr}f_{tr} + \delta_{ev}f_{ev} + \delta_{adv}f_{adv} , \tag{11}$$

$$f_{ev} + f_{tr} + f_{adv} = 1 , \tag{12}$$

Where f_{tr}, f_{ev} and f_{adv} are the proportional contributions of transpiration, surface evaporation and advection to precipitation, respectively, The f values of three kinds of water vapor were obtained by ISOSource software (https://www.epa.gov/) (Phillips & Gregg, 2001). δ_{pv}, δ_{tr}, δ_{ev} and δ_{adv} represent the stable isotopic compositions of precipitation vapor, vegetation transpiration vapor, water-surface evaporation vapor, and advected vapor, respectively. δ_{pv} is calculated using the following formula:

$$\delta_{pv} = \frac{\delta_p - k\varepsilon^+}{1 + k\varepsilon^+} , \tag{13}$$

Where δ_p represents the stable isotopic composition of precipitable liquid water.

Based on the isotopic relationships among different water phases in either open or closed isotope systems, we use the isotope evaporation model proposed by Craig and Gordon (1965) to determine the stable isotopic composition of soil evaporation vapor (δ_{ev}). The equation is as follows:

$$\delta_{ev} = \frac{\delta_s/\alpha^+ - h\delta_{adv} - \varepsilon}{1 - h + \varepsilon_k} , \tag{14}$$

Including the δ_S is the isotopic composition of liquid water evaporation front, δ_{adv} is advective vapor, h is relative humidity, α^+ is equilibrium fractionation factor, ε_k is kinetic fractionation factor, ε is total fractionation factor.

$$\varepsilon = \varepsilon^+/\alpha^+ + \varepsilon_k , \tag{15}$$

$$\varepsilon_k = (1 - h)\theta_n C_k , \tag{16}$$

h is the relative humidity, C_k is the kinetic fractionation constant, δ^2H is 25.1‰, $\delta^{18}O$ is 28.5‰.The weight coefficient θ of small water body is 1, and θ of large water body is 0.5. n ranges from 0.5 (fully turbulent transport, with reduced kinetic

fractionation, suitable for lake or saturated soil conditions) to 1 (fully diffused transport, suitable for very dry soil conditions), with a kinetic fractionation coefficient of about 12.2-24.5‰ for ε_k (^{2}H) in a dry atmosphere (h=0). The kinetic separation coefficient of ε_k (^{18}O) is about 13.8-27.7‰.

The advection water vapor isotope δ_{adv} in the three-component mixing model needs to be determined by the water vapor isotopic composition at the upwind position. The HYSPLIT model (http://www.arl.noaa.gov/ready/HYSPLIT.html), designed for atmospheric transport analysis using gridded meteorological data, was applied to track moisture sources and analyze air mass trajectories to sampling locations (Stein et al., 2015). We found that the northeastern of Tibetan Plateau was controlled by westerly winds, southeast monsoon and plateau monsoon in June, July and August, and by prevailing westerly winds in September and October. The clustering analysis of air masses in different months shows that air masses accumulate at the northern foot of Qilian Mountains and move from low altitude to high altitude along the valley. Xiying, at 2097 m above sea level, is therefore used as a upwind station from April to October(Zhang et al., 2021). As the air mass ascends along the elevation gradient from this station, the isotope of advective vapor is progressively depleted. Notably, although recycled vapor produced by evapotranspiration does enter the air mass to some extent, most of it escapes to other regions without contributing to precipitation. Consequently, its influence on advective vapor downwind can be considered negligible (Li & Zhang, 2003; Wang et al., 2016). Because this transport process is irreversible and departs from isotopic mass balance in the atmosphere, isotopic fractionation is assumed to be due to Rayleigh distillation(Peng et al., 2011), which is formulated as follows:

$$\delta_{adv} = \delta_{pv-adv} + (\alpha^+ - 1)\ln F , \tag{17}$$

Where δ_{pv-adv} denotes the isotopic composition of precipitable water vapor at the upwind station, which is obtained from Equation (13). The parameter F primarily reflects atmospheric moisture conditions during regional precipitation formation and is commonly represented by the ratio of final to initial water vapor. Since water vapor content is positively correlated with the surface vapor pressure of the whole study area (c=1.657e, where c is the water vapor content in mm, e is the surface vapor pressure in hPa, R^2=0.94) (Hu et al., 2015), the surface vapor pressure of each site was used to calculate the value of F.

4 Results and analysis

### 4.1 Hydrogen and oxygen isotope variations in different water bodies

During the growth season of Picea crassifolia, precipitation stable isotopes display distinct fluctuation patterns(Table 2). In the initial growth phase, the hydrogen and oxygen isotope ratios exhibit relatively low values. With the progressive rise in temperature, the rate of water evaporation and subsequent loss escalates, resulting in an isotopic enrichment. The mean δ^2H value in precipitation throughout the growth season is recorded at -45.52‰, with fluctuations ranging from -151.88‰ to 63.43‰. Similarly, the mean δ^{18}O value stands at -7.75‰, exhibiting fluctuations between -31.49‰ and 14.79‰. The isotopic composition in the wood tissues does not show significant depletion or enrichment, displaying a fluctuation range from -76.95‰ to 23.87‰ for δ^2H and from -11.92‰ to 24.77‰ for δ^{18}O. Compared to precipitation and wood tissues,

shallow soil water demonstrates a lesser enrichment of heavy isotopes, with a reduced fluctuation extent observed during the late spring and early summer period.

Table 2:Stable isotopes of different water bodies during the growing season.

| Average Period	δ²H/‰			δ¹⁸O/‰		
	Precipitation	Xylem water	Soil water（0~10cm）	Precipitation	Xylem water	Soil water（0~10cm）
April	-69.15	-39.02	-53.10	-10.25	2.56	-7.10
May	-39.09	-29.78	-45.38	-7.61	4.44	-6.42
June	-31.29	-45.83	-46.08	-5.74	-2.83	-6.12
July	-32.39	-47.63	-47.71	-5.33	-0.97	-7.06
August	-48.88	-44.55	-68.85	-7.79	-2.06	-9.07
September	-29.38	-42.62	-49.20	-6.46	-1.83	-6.79
October	-68.43	-44.57	-54.88	-11.06	-2.25	-7.96

Using the Global Meteoric Water Line (GMWL) as a reference standard, regional water lines are influenced by factors like moisture source and re-evaporation during precipitation. The intersection points of the Local Meteoric Water Line (LMWL), Soil Water Line (SWL), and Local Evaporation Line (LEL) can reveal recharge relationships between different water bodies. Their slopes reflect key information including local temperature and humidity characteristics, and the degree of evaporative fractionation in water bodies. Variations in the Local Meteoric Water Line (LMWL) across different vertical gradients are primarily influenced by temperature and humidity. Notably, relative humidity remains consistently low at all four measured elevations within the forest, causing the LMWL to be lower than the Global Meteoric Water Line (GMWL). At an elevation of 2543 meters, which marks the lowest tree growth layer, temperatures can reach up to 20℃ in July, with the LMWL showing a slope of 6.74. At 2721 meters, the average temperature during the growing season is 10.4℃, peaking at 16.45℃ in July and an average relative humidity of 64.38%. The slope of the LMWL at this elevation is 7.02(Figure 2d). At the Suidao station, located at an elevation of 3448 meters, the slope of the precipitation regression line is 7.75. This value is close to the GMWL's slope but exhibits the largest deviation from the local evaporation line, as depicted in (Figure 2a). In the forest's lower layer, the Soil Water Line (SWL) is narrower and closer to the local evaporation line, indicating more pronounced evaporative fractionation and dynamic fractionation compared to the other three sampling zones. The SWL slopes are less steep than those of the LMWL, indicating that precipitation is the primary source of soil moisture replenishment.
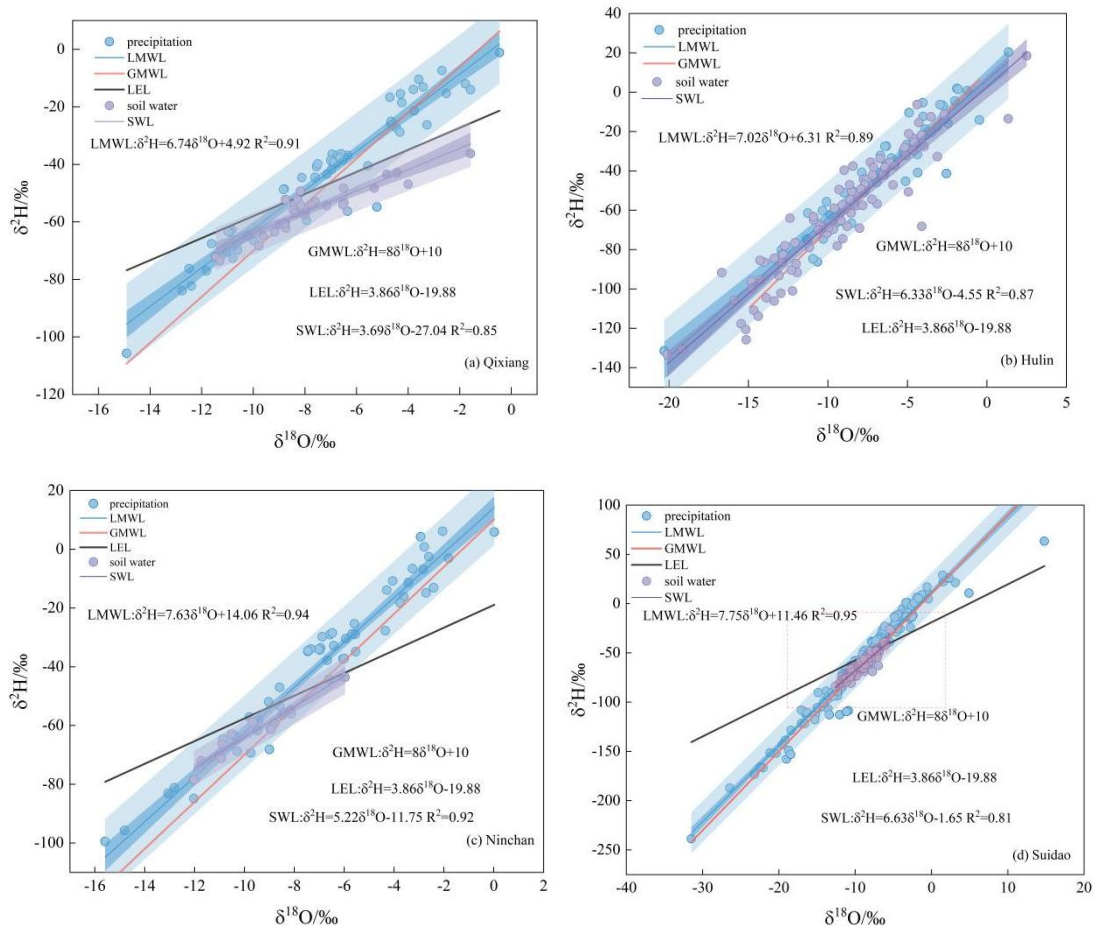
Figure 2:(a) Qixiang, (b) Hulin, (c) Ninchan, (d) Suidao. Compare the distributions and fittings of precipitation and soil water stable isotopes at the four locations.

The d-excess parameter measures how much precipitation deviates from the Global Meteoric Water Line, reflecting the impact of re-evaporation on isotope fractionation. Higher d-excess values indicate stronger non-equilibrium evaporation during regional moisture transport. During the precipitation process, unsaturated water vapor leads to non-equilibrium fractionation, as indicated by an average d-excess value of 16.58‰ throughout the growing season (Figure 3a). Lower relative humidity in May and September resulted in higher d-excess values compared to other months, indicating more pronounced non-equilibrium evaporation during precipitation events. From June to August, the fluctuations in deuterium values are gradual; however, significant variations begin from mid-August onwards. This trend suggests that local evaporation intensifies over time, influenced by temperature and relative humidity, resulting in increased rates of non-equilibrium evaporation. At higher elevations, the soil moisture content across all soil layers remains above 30%, influenced by rainfall and snowmelt (Figure 3b). By the end of the growing season, decreasing temperatures lead to leaf fall, resulting in

11

the formation of a litter layer on the forest floor. This layer plays a pivotal role in retaining soil moisture, underscoring the dynamic interactions between vegetation, soil, and atmospheric conditions throughout the season.

270
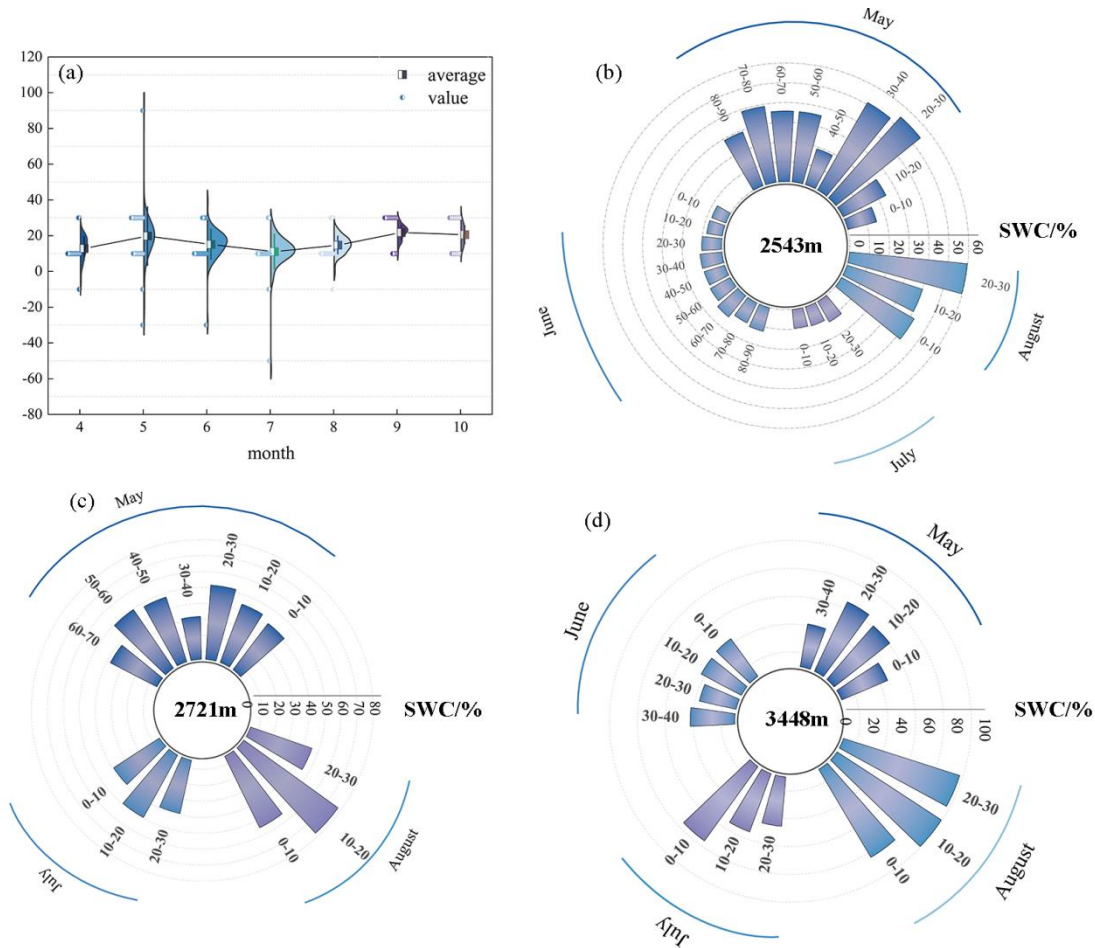
Figure 3: (a) The average variation of d-excess during the growing season within the gradient of 2543 to 3448 m; (b), (c), and (d) represent the soil moisture content at different depths at elevations of 2543 m, 2721 m, and 3448 m, respectively.

## 4.2 Soil evaporation, plant transpiration and ecosystem evapotranspiration

Table 3: The isotopic composition of vegetation transpiration(δ_T), soil evaporation(δ_E), and ecosystem evapotranspiration(δ_{ET}) at
275 **different elevations during the growing season(* represents missing value).**

Site	Type	April	May	June	July	August	September	October
	δ_T	2.22	-5.87	-4.59	-0.72	-1.72	-1.78	-2.26
Qixiang	δ_E	-30.32	-28.68	-27.33	-29.12	-28.68	-26.32	-27.27
	δ_{ET}	-20.19	-20.05	-11.63	-9.87	-13.56	-15.85	-21.56
	δ_T	-5.34	-3.58	-4.13	-0.34	-2.35	-4.25	-1.97
Hulin	δ_E	-29.68	-27.28	-25.8	-27.75	-24.56	-25.21	-27.88
	δ_{ET}	-21.59	-22.36	-8.93	-10.17	-11.57	-18.8	*

12

Ninchan	δ_T	*	-3.45	-1.98	-1.05	-6.68	*	*
	δ_E	*	-20.57	-26.31	-29.08	-18.22	-18.15	-18.22
	δ_{ET}	*	*	-12.46	-7.57	*	*	*
Suidao	δ_T	*	-8.45	-6.98	-6.05	-6.68	*	*
	δ_E	-29.79	-27.32	-27.91	-23.83	-28.78	-25.8	-28.06
	δ_{ET}	-24.31	-16.14	-15.19	-10.07	-18.05	-23.02	-18.65

The Keeling plot method was used to analyze the stable isotope composition of ecosystem evapotranspiration (Figure 4). Its principle involves linearly fitting the water vapor concentration in the ecosystem boundary layer against the oxygen isotope composition, with the intercept on the y-axis representing the stable isotope value of δ_{ET}. The results indicate that at different heights within the distribution of deciduous trees, the average δ_{ET} value is -22.59‰. Throughout the entire growing season,

280 δ_{ET} does not consistently decrease with increasing elevation. Specifically, near the treeline, there are higher stable isotope values, but in the middle and upper layers of the forest, there is a minimal value, indicating lower and less stable isotopic fractionation in that layer. At an elevation of 3448m, as the number of deciduous trees decreases and shrubs become dominant, the δ_{ET} value is -21.81‰(Table 3). We found that the stable isotope δ_E of soil evaporation at depths of 0-10cm is more enriched at lower elevations, particularly in April and May when the isotopic enrichment is more pronounced. From

285 June to August, due to a significant increase in vegetation coverage, soil evaporation intensity decreases. In the early stage of the growing season, when leaves have not fully developed, the stable isotope composition of the xylem exhibits a relatively depleted characteristic. In July and August, when leaves are fully expanded, temperatures rise, and the rainy season in mountainous areas commences, transpiration becomes more intense.


(a)Qixiang: $y=148.60x-21.76$ $R^2=0.26$ $P<0.01$

(b)Hulin: $y=235.80x-21.70$ $R^2=0.25$ $P<0.01$
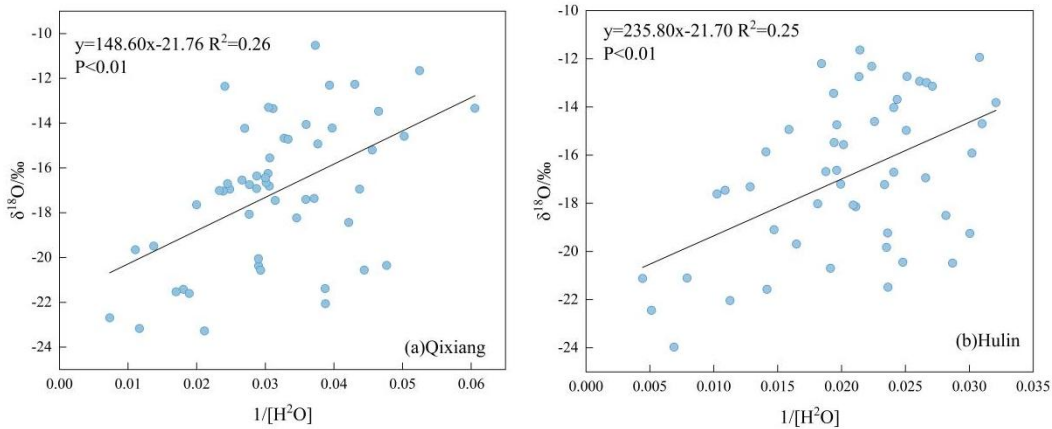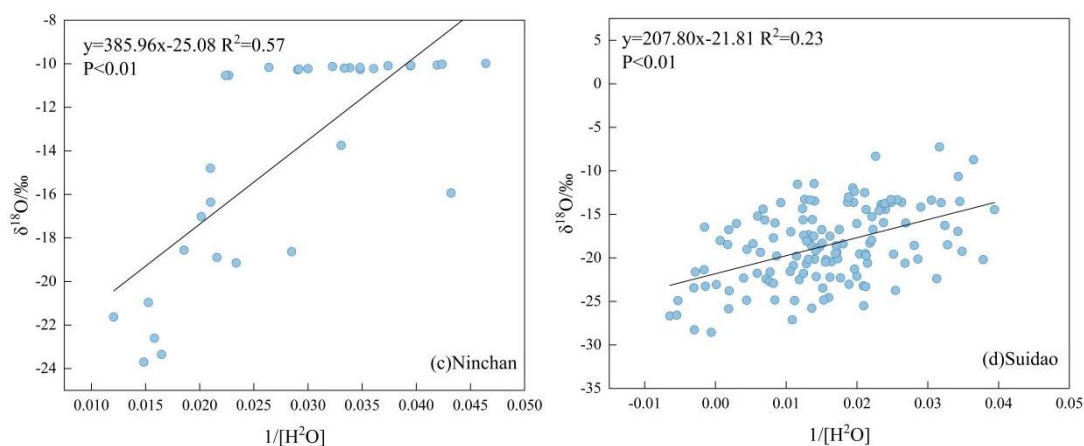
Figure 4:Each sampling point is fitted with a trend line based on the Keeling plot method.

4.3 T/ET assessment of Picea crassifolia ecosystem in different months

We found that the canopy closure of deciduous trees significantly influences the evapotranspiration of the entire ecosystem (Figure 5). In April and May, as temperatures rise, surface vegetation exhibits weaker growth, resulting in a higher proportion of soil evaporation within the ecosystem, while transpiration by vegetation remains relatively low. During the rainy season in June to August, vegetation experiences vigorous growth, and transpiration reaches its peak in July. In September and October, soil evaporation becomes more dominant as temperatures, relative humidity, and rainfall gradually decrease, and deciduous tree leaves become wilted. At lower elevations, the T/ET ratio fluctuates between 0.20 and 0.70 in a different pattern, while above the treeline, transpiration ratios fluctuate between 0.20 and 0.80 in a similar pattern. Overall, summer is characterized as the peak season for transpiration, with a minimal contribution from soil evaporation.

14
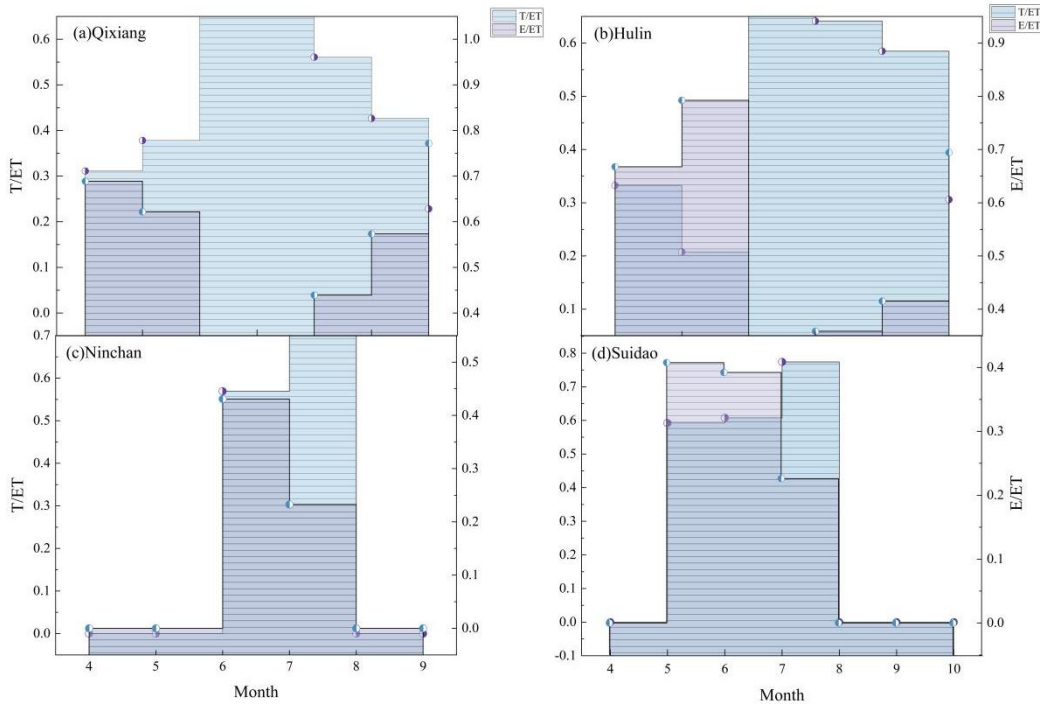
Figure 5:(a), (b), (c), and (d) represent the proportion of soil evaporation and vegetation transpiration in the evapotranspiration of the ecosystem at different sampling points (0 represents a missing value).

5 Discussions

5.1 Hydrological effects of changes in evapotranspiration

The analysis results indicate that the proportion of vegetation in ecosystem evapotranspiration and recycled water vapor is significantly greater than that of the soil. Furthermore, the enhanced evapotranspiration capacity accelerates the cycling rate of water vapor, promoting precipitation formation. Within the altitude gradient of 2700-3000 m, the contribution of advected water vapor gradually declines (Table S1), while the contribution ratio of recycled water vapor to precipitation gradually increases (Figure 7). This is attributed to relatively high temperatures in the lower layers of the forest and the dense presence of Picea crassifolia in the middle to upper layers, resulting in a higher transpiration ratio (f_{tr}) throughout the entire growing season. In July, which typically experiences higher temperatures and increased vegetation activity, the ratio of vegetation transpiration(f_{tr}) is significantly higher compared to other months. Both the early and late stages of the growing season exhibit noticeably higher evaporation ratios (f_{ev}) compared to other months, with the middle and upper parts of the forest having a greater proportion of evaporated vapor. The average advected vapor ratio (f_{adv}) is 72%, with contributions exceeding 70% for all months except June and July. In mountainous areas, recycled water vapor contributes an average of 28% to precipitation, indicating that the increase in evapotranspiration promotes the occurrence of local precipitation events.

15

This also means that cross-regional water vapor transport and local-scale recycled water vapor alleviate regional water resource crises and enhance the ecosystem's resilience to drought by regulating the redistribution of precipitation and surface water (Quan et al., 2024).
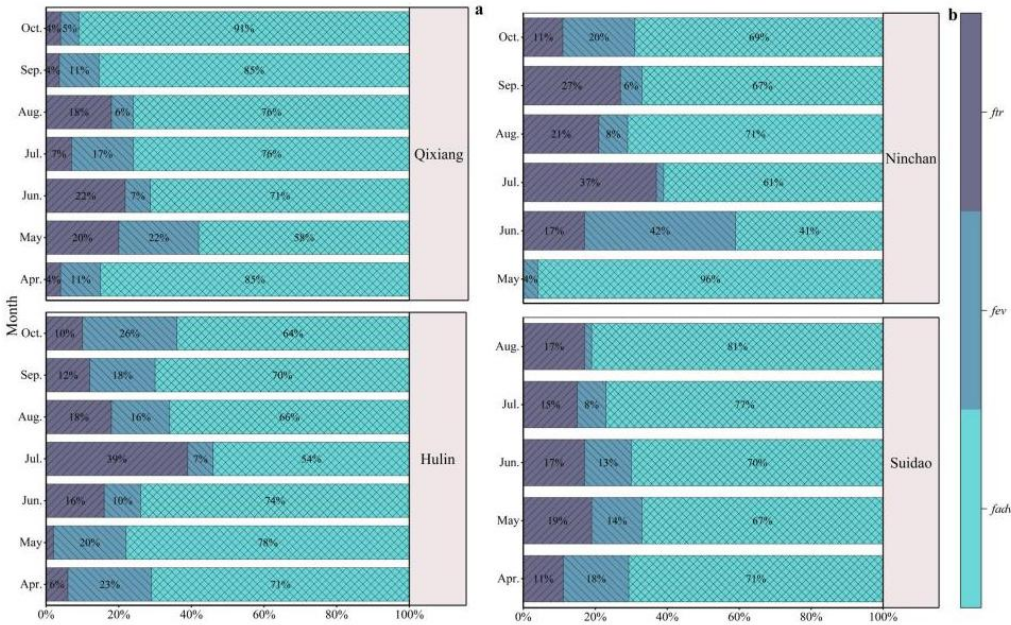
Figure 7:Comparison of f_{adv} (advective water vapour contribution), f_{ev} (surface evaporation water vapour contribution) and f_{tr} (plant transpiration water vapour contribution) for each of period.

5.1.2 Impact on surface runoff

The formation of runoff is regulated by elevation. In the distribution area of Picea crassifolia, the level of evapotranspiration is much higher than precipitation, making it difficult for surface runoff to form. Comparing the differences of monthly potential evapotranspiration, surface evapotranspiration and precipitation in Picea crassifolia (Table 4), the results clearly showed that rainfall fluctuated between 0-16mm, and the maximum rainfall was 15.7 mm in April, while the minimum value of surface evapotranspiration is 41.8 mm and the minimum value of potential evapotranspiration is 44.1mm. The difference between ET_P and ET shows that there is no effective water accumulation in all months. Between 2500 m and 3400 m, Picea crassifolia-dominated forests cover approximately 38.5% of the watershed area. However, such vegetation exerts only a minor influence on total annual runoff (He et al., 2012). With rising temperatures, precipitation becomes the primary water source for these forests, whereas during dry and cold seasons, snowmelt and seasonal permafrost are integral for both forest water supply and baseflow formation. Seasonal permafrost above 3000 m shapes baseflow from November through April. Over the growing season (2700－3400 m), rainfall is the governing factor behind runoff dynamics (Liu et al., 2023), and snowmelt accounts for 33% of the water absorbed by Picea crassifolia (Zhu et al., 2022). Overall, forests at mid-elevation largely rely on rainfall, secondarily on meltwater and seasonal permafrost, while their ability to intercept rainwater for runoff

generation is relatively limited. Notably, the thickness of seasonal permafrost in this region has declined by 7.4 cm per decade (Qin et al., 2016), further restricting its influence on runoff. From this, an important conclusion can be drawn: at elevations between 2500 m and 3400 m, local evapotranspiration substantially exceeds precipitation. Regional runoff is predominantly sustained by precipitation, with forest interception and seasonal permafrost having limited effects on runoff. The feeble runoff generation potential in this region also indicates that afforestation would significantly increase water loss via ET, posing a threat to water distribution and utilisation.

Table 4:Variations in evapotranspiration(ET) and precipitation(P) across different elevation zones during april to october.

Altitide/m	Parameters	April	May	June	July	August	September	October	Data Sources
2700	ET/mm	51.5	66.3	93.3	108.9	110.7	81.2	41.8	(Yao et al., 2017)
2700	P/mm	29	31.2	103.5	90.3	66.9	39.3	10.4	（Zhao et al., 2019;2020）
3200	ET/mm	37.5	90	95	107.5	107.5	65	65	(Yang et al., 2019)
3200	P/mm	27.9	43.9	62.3	39.4	56.6	42.7	23.6	（Zhao et al., 2021;2022）

Some studies suggested that reducing forest density will result in less ET in seasonally dry forests. That reduced ET can be converted into increased groundwater and runoff to supply downstream social water (Wyatt, O'Donnell, & Springer, 2015). It has also been claimed that in some cases, the transient increase in water availability through reduced forest density can actually contribute to subsequent increases in vegetation cover and ultimately reduce runoff (Tague et al., 2019). By assessing the hydrological effects of afforestation through the water cycle in the Asia-Pacific region, it was found that in 7 of the 15 water-deficient areas, positive effects such as increased yield, precipitation, soil moisture and reduced drought risk were achieved through afforestation, and it was confirmed that the water-water cycle had a strong impact and evapotranspiration was increased (Teo et al., 2022). The water vapour content produced by forest transpiration is much higher than that lost by soil surface evaporation, most of the precipitation is intercepted and infiltrated by surface vegetation, and part of the soil water involved in infiltration is absorbed by the root zone of vegetation. Because of plants' high interception and evaporation ability and the absorption of groundwater by root zone, the proportion of transpiration was significantly higher than that of evaporation(Su et al., 2014). In this study zone, upwardly transported advective water vapor progressively diminishes with increasing altitude. The vegetation at elevations from 2500 to 3200 meters supplies abundant evapotranspiration water vapor into the water cycle, the acceleration of which boosts local precipitation(Figure 6). Within the elevation range of 2543 to 3448 m, precipitation and seasonal permafrost are the main sources of groundwater recharge.

Over the past 55 years, the seasonal permafrost has decreased at a rate of about 7.4 cm per decade (Li et al., 2016). Correlation analysis shows that when seasonal permafrost decreases, soil moisture in the upper layer increases (Qin et al., 2016). As vegetation transpiration increasingly consumes precipitation, soil water, and groundwater, the remaining groundwater becomes more limited. Consequently, within this elevation range, the contribution of groundwater to runoff formation is minimal.
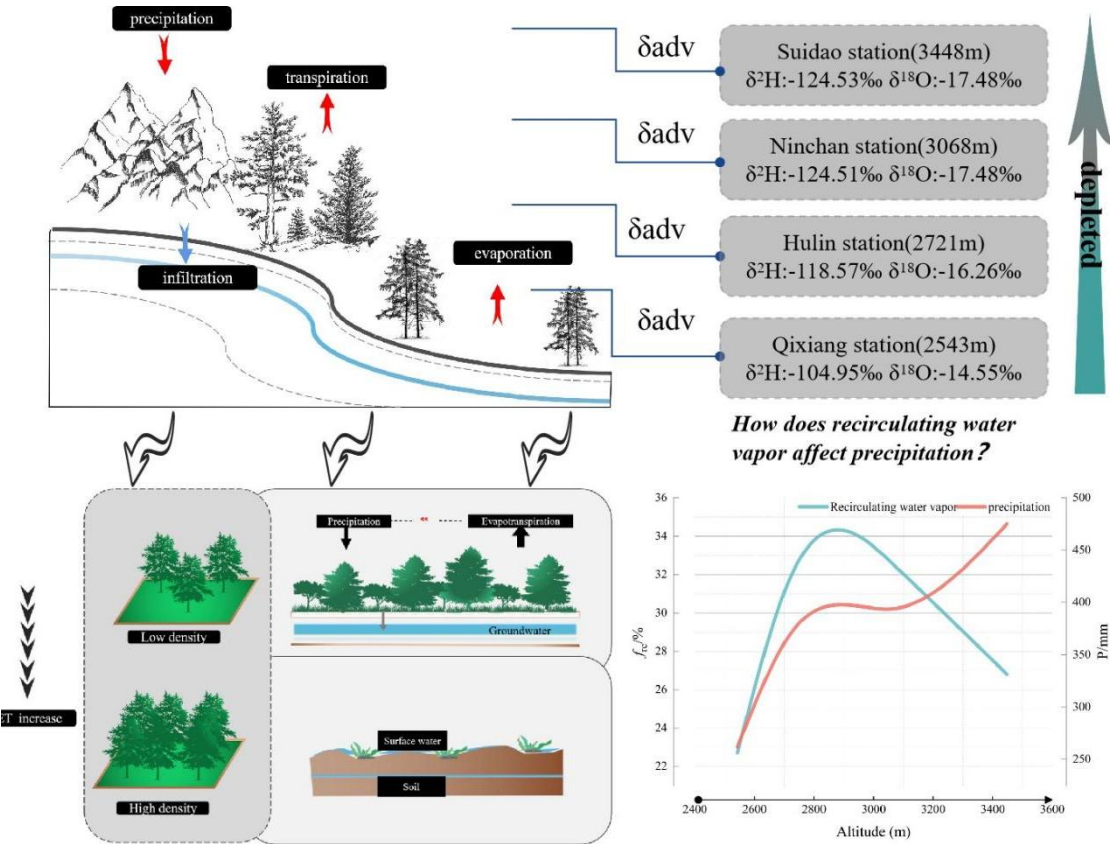

Figure 6:Conceptual model of the hydrological effects of changes in evapotranspiration.

5.2 Uncertainty analysis

A higher sample size can reduce the margin of error. Therefore, we utilized isotopic data from four sites over a two-year period to evaluate the model. We used 404 xylem samples to calculate the contribution ratio of transpiration to ecosystem evapotranspiration. We examined the uncertainty of the model evaluation. When analyzing the evaporation characteristics in a semi-arid natural environment using the Craig-Gordon isotopic model, we first eliminated the influence of solar radiation and other meteorological variables on the calculation results. We focused on temperature, relative humidity, water vapor, and the initial isotopic values of water bodies. Particularly in semi-arid environments, the variations in temperature and relative

18

humidity are crucial (Hernández-Pérez et al., 2020). To verify the calculation results, we found a strong correlation between the isotopes of soil evaporation and relative humidity, as demonstrated by the fitting of δ_E against relative humidity and temperature(Figure 8). This also indicates the reliability of the results obtained through the Craig-Gordon isotopic model. We employed the Keeling plot method to calculate δ_{ET}, which is based on isotopic mass balance and a two-endmember mixing model. This method assumes that the isotopic composition of the background atmosphere and source remains constant, with a very low probability of isotopic spatial variation (Good et al., 2012; Kool et al., 2014). Due to the higher reliability of oxygen isotopes compared to hydrogen isotopes (Han et al., 2022; Kale et al., 2022), we solely used oxygen isotopes to calculate the T/ET values. The results indicate that transpiration significantly outweighs evaporation during July and August, which aligns with previous research findings (Zhu et al., 2022). The correlation between T/ET and soil moisture content suggests that soil moisture is a crucial factor driving the variations in transpiration and evaporation ratios. Additionally, the estimation of isotopic composition of advected water vapor from the upwind sites contributes to increased uncertainty. In our study area, the sites are predominantly influenced by valley winds, with water vapor moving from the valley bottom to higher altitudes. Therefore, we selected lower elevation areas in the valley bottom as the source region for advected water vapor (Zhang et al., 2021).
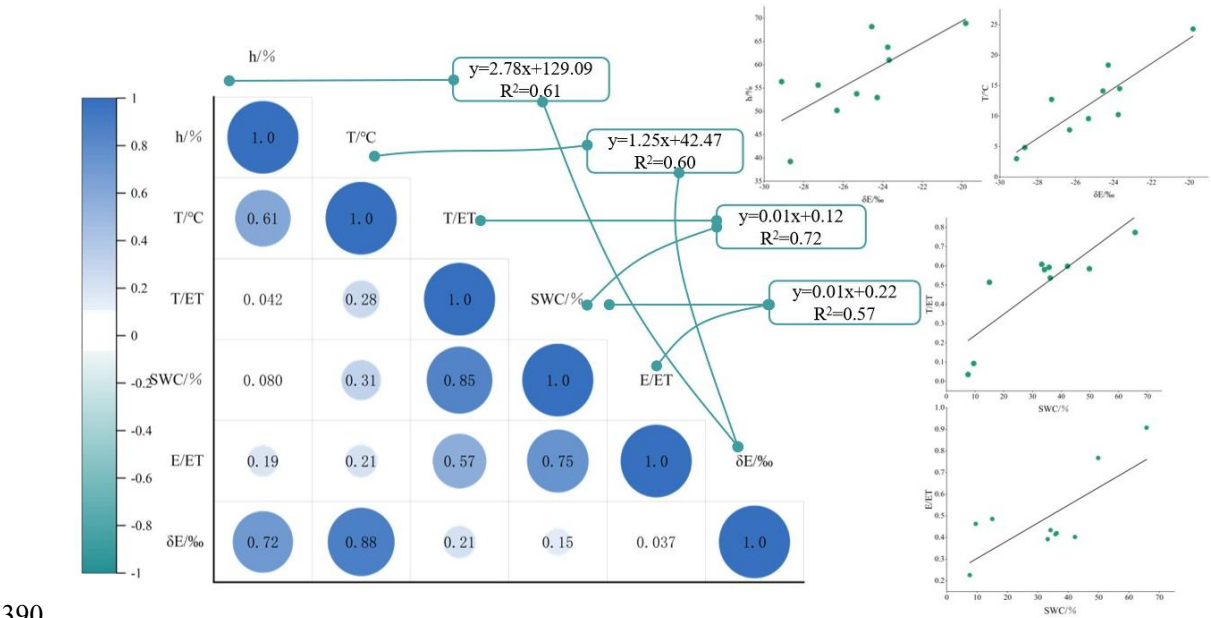
Figure 8:Correlation analysis of factors affecting uncertainty in impact assessment.

6 Conclusions

This study leverages isotopic data from field observations (2018-2022) and model simulations to investigate the dynamics of evapotranspiration in the northeastern Tibetan Plateau, aiming to elucidate its relationship with local water cycling and

395 hydrological impacts. The findings reveal that evaporation and transpiration rates peak during July and August, indicating that transpiration from Picea crassifolia plays a more dominant role than soil evaporation in these periods. Quantitative analysis of plant transpiration and soil evaporation contributions to total evapotranspiration yielded an average T/ET ratio of 0.57 over the study period, reaching a maximum of 0.77 in July. Consequently, it is evident that transpiration by forest trees is the primary component of evapotranspiration within the Picea crassifolia ecosystem. Further examination of the

400 hydrological effects associated with Picea crassifolia evapotranspiration demonstrates that monthly evapotranspiration volumes are at least threefold higher than precipitation, significantly limiting the potential for surface runoff formation in this region. Comparative analysis of atmospheric water vapor contributions from precipitation across spring, summer, and autumn reveals that the June to August period marks the peak transpiration season for Picea crassifolia, contributing up to 25% of total atmospheric water vapor, whereas surface evaporation accounts for only 18%. Within the 2543 to 3448m

405 elevation range,the average value of f_{re} is 28%, it is indicated that the water vapor cycle generated by vegetation evapotranspiration has increased the total precipitation in high-altitude mountain areas. In light of global warming, drought, water scarcity, and climate changes driven by relative humidity alterations have significantly impacted the ecological communities, ecosystem functions, services, and land-climate interactions of Picea crassifolia. It is imperative to recognize the critical role of evapotranspiration in depleting rainfall within this forest belt, underscoring its significance for local water

410 resource management and ecological conservation.

Data availability

The data that support the findings of this study are available on request from the corresponding author, stable isotope data are not publicly available due to privacy or ethical restrictions. Precipitation and surface evapotranspiration data are available from the National Tibetan Plateau Scientific Data Centre(TPDC).

415 **Author contribution**

Yinying Jiao and Guofeng Zhu conceived the idea of the study; Gaojia Meng, Siyu Lu analyzed the data; Dongdong Qiu, Qinqin Wang, Rui Li, Longhu Chen participated in the drawing; Yinying Jiao wrote the paper; Wentong Li checked the format. All authors discussed the results and revised the manuscript.

Competing interests

420 The authors declare that they have no conflict of interest.

Acknowledgements

References

An, Q., Liu, L., Wang, L., Yang, K., Cheng, Y., Liu, J., and Huang, G.: Contribution of moisture recycling to water availability in China, Water Resour. Res., 61(4), doi:10.1029/2024wr038054, 2025.

Aron, P. G., Poulsen, C. J., Fiorella, R. P., Matheny, A. M., and Veverica, T. J.: An isotopic approach to partition evapotranspiration in a mixed deciduous forest, Ecohydrology, 13, doi:10.1002/eco.2229, 2020.

Ault, T. R.: On the essentials of drought in a changing climate, Science, 368, 256–260, doi:10.1126/science.aaz5492, 2020.

Brubaker, K. L., Entekhabi, D., and Eagleson, P. S.: Estimation of continental precipitation recycling, J. Climate, 6, 1077–1089, doi:10.1175/1520-0442(1993)006, 1993.

Celik, S. K., Madenoglu, S., and Turker, U.: Partitioning evapotranspiration of winter wheat based on oxygen isotope approach under different irrigation regimes, Irrig. Drain., 71, 882–896, doi:10.1002/ird.2701, 2022.

Cheng, T. F., Chen, D., Wang, B., Ou, T., and Lu, M.: Human-induced warming accelerates local evapotranspiration and precipitation recycling over the Tibetan Plateau, Commun. Earth Environ., 5(1), doi:10.1038/s43247-024-01563-9, 2024.

Craig, H., and Gordon, L. I.: Deuterium and oxygen 18 variations in the ocean and the marine atmosphere, In E. Tongiorgi (Ed.), Stable isotopes in oceanographic studies and paleotemperatures, 9–130, 1965.

Cui, J., Lian, X., Huntingford, C., Gimeno, L., Wang, T., Ding, J., et al.: Global water availability boosted by vegetation-driven changes in atmospheric moisture transport, Nat. Geosci., 15, 982–988, doi:10.1038/s41561-022-01061-7, 2022.

Dansgaard, W.: Stable isotopes in precipitation, Tellus, 16, 436–468, doi:10.1111/j.2153-3490.1964.tb00181.x, 1964.

Ding, Y. and Peng, S.: Spatiotemporal change and attribution of potential evapotranspiration over China from 1901 to 2100, Theor. Appl. Climatol., 145, 79–94, doi:10.1007/s00704-021-03625-w, 2021.

Ding, Y. and Peng, S.: Spatiotemporal Trends and Attribution of Drought across China from 1901–2100, Sustainability, 12, 477, doi:10.3390/su12020477, 2020.

Eisenhauer, N., and Weigelt, A.: Ecosystem effects of environmental extremes, Science, 374, 1442 – 1443, doi:10.1126/science.abn1406, 2021.

Evaristo, J., Jasechko, S., and McDonnell, J. J.: Global separation of plant transpiration from groundwater and streamflow, Nature, 525, 91–94, doi:10.1038/nature14983, 2015.

Farquhar, G. D., Cernusak, L. A., and Barnes, B.: Heavy water franctionation during transpiration, Plant Physiol., 143, 11–18, doi:10.1104/pp.106.093278, 2007.

Gibson, J. J. and Reid, R.: Stable isotope fingerprint of open-water evaporation losses and effective drainage area fluctuations in a subarctic shield watershed, J. Hydrol., 381, 142–150, doi:10.1016/j.jhydrol.2009.11.036, 2009.

Gibson, J. J. and Reid, R.: Water balance along a chain of tundra lakes: A 20-year isotopic perspective, J. Hydrol., 519, 2148–2164, doi:10.1016/j.jhydrol.2014.10.011, 2014.

Good, S. P., Soderberg, K., Wang, L., and Caylor, K. K.: Uncertainties in the assessment of the isotopic composition of surface fluxes: A direct comparison of techniques using laser-based water vapor isotope analyzers, J. Geophys. Res. Atmos., 117, doi:10.1029/2011jd017168, 2012.

Han, J., Tian, L., Cai, Z., Ren, W., Liu, W., Li, J., and Tai, J.: Season-specific evapotranspiration partitioning using dual water isotopes in a Pinus yunnanensis ecosystem, southwest China, J. Hydrol., 608, 127672, doi:10.1016/j.jhydrol.2022.127672, 2022.

Hao, L., Sun, G., Huang, X., Tang, R., Jin, K., Lai, Y., et al.: Urbanization alters atmospheric dryness through land evapotranspiration, npj Clim. Atmos. Sci., 6, doi:10.1038/s41612-023-00479-z, 2023.

He, Z., Zhao, W., Liu, H., and Tang, Z.: Effect of forest on annual water yield in the mountains of an arid inland river basin: a case study in the Pailugou catchment on northwestern China's Qilian Mountains, Hydrol. Process., 26, 613–621, doi:10.1002/hyp.8162, 2011.

Hernández-Pérez, E., Levresse, G., Carrera-Hernández, J., and García-Martínez, R.: Short term evaporation estimation in a natural semiarid environment: New perspective of the Craig – Gordon isotopic model, J. Hydrol., 587, 124926, doi:10.1016/j.jhydrol.2020.124926, 2020.

Horita, J., and Wesolowski, D. J.: Liquid-vapor fractionation of oxygen and hydrogen isotopes of water from the freezing to the critical temperature, Geochim. Cosmochim. Acta, 58, 3425–3437, doi:10.1016/0016-7037(94)90096-5, 1994.

Hu, W.-F., Yao, J.-Q., He, Q., and Yang, Q.: Spatial and temporal variability of water vapor content during 1961–2011 in Tianshan Mountains, China, J. Mt. Sci., 12, 571–581, doi:10.1007/s11629-014-3364-y, 2015.

Keeling, C. D.: The concentration and isotopic abundances of atmospheric carbon dioxide in rural areas, Geochim. Cosmochim. Acta, 13, 322–334, doi:10.1016/0016-7037(58)90033-4, 1958.

Kong, Y., Pang, Z., and Froehlich, K.: Quantifying recycled moisture fraction in precipitation of an arid region using deuterium excess, Tellus B, 65, 19251, doi:10.3402/tellusb.v65i0.19251, 2013.

Kool, D., Agam, N., Lazarovitch, N., Heitman, J. L., Sauer, T. J., and Ben-Gal, A.: A review of approaches for evapotranspiration partitioning, J. Adv. Res., 184, 56–70, doi:10.1016/j.agrformet.2013.09.003, 2014.

Li, X. and Zhang, G.: Research on Precipitable Water and Precipitation Conversion Efficiency around Tianshan Mountain Area, J. Desert Res., 23, 509–513, 2003.

Li, Z., Feng, Q., Wang, Q. J., Song, Y., Li, H., and Li, Y.: The influence from the shrinking cryosphere and strengthening evopotranspiration on hydrologic process in a cold basin, Qilian Mountains, Glob. Planet. Change, 144, 119 – 128, doi:10.1016/j.gloplacha.2016.06.017, 2016.

Li, Zhao, Ciais, P., Wright, J. S., Wang, Y., Liu, S., Wang, J., et al.: Increased precipitation over land due to climate feedback of large-scale bioenergy cultivation, Nat. Commun., 14, doi:10.1038/s41467-023-39803-9, 2023.

Li, Zongxing, Yuan, R., Feng, Q., Zhang, B., Lv, Y., Li, Y., et al.: Climate background, relative rate, and runoff effect of multiphase water transformation in Qilian Mountains, the third pole region, Sci. Total Environ., 663, 315 – 328, doi:10.1016/j.scitotenv.2019.01.339, 2019.

Liu, Y., Kumar, M., Katul, G. G., Feng, X., and Konings, A. G.: Plant hydraulics accentuates the effect of atmospheric moisture stress on transpiration, Nat. Clim. Change, 10, 691–695, doi:10.1038/s41558-020-0781-5, 2020.

Liu, Y., Lian, J., Luo, Z., and Chen, H.: Spatiotemporal variations in evapotranspiration and transpiration fraction following changes in climate and vegetation in a karst basin of southwest China, J. Hydrol., 612, 128216, doi:10.1016/j.jhydrol.2022.128216, 2022.

Liu, Y., Zhuang, Q., Miralles, D., Pan, Z., Kicklighter, D., Zhu, Q., et al.: Evapotranspiration in Northern Eurasia: Impact of forcing uncertainties on terrestrial ecosystem model estimates, J. Geophys. Res. Atmos., 120, 2647 – 2660, doi:10.1002/2014jd022531, 2015.

Liu, Z., Wang, N., Cuo, L., and Liang, L.: Characteristics and attribution of spatiotemporal changes in Qilian Mountains' runoff over the past six decades, J. Geophys. Res. Atmos., 128, doi:10.1029/2023jd039176, 2023.

Makarieva, A. M., Nefiodov, A. V., Nobre, A. D., Baudena, M., Bardi, U., Sheil, D., et al.: The role of ecosystem transpiration in creating alternate moisture regimes by influencing atmospheric moisture convergence, Glob. Change Biol., 29, 2536–2556, doi:10.1111/gcb.16644, 2023.

Maxwell, R. M. and Condon, L. E.: Connections between groundwater flow and transpiration partitioning, Science, 353, 377–380, doi:10.1126/science.aaf7891, 2016.

Mehmood, S., Ashfaq, M., Kapnick, S., Gosh, S., Abid, M. A., Kucharski, F., et al.: Dominant controls of cold-season precipitation variability over the high mountains of Asia, npj Clim. Atmos. Sci., 5, doi:10.1038/s41612-022-00282-2, 2022.

Peng, S., Ding, Y., Liu, W., and Li, Z.: 1 km monthly temperature and precipitation dataset for China from 1901 to 2017, Earth Syst. Sci. Data, 11, 1931–1946, doi:10.5194/essd-11-1931-2019, 2019.

Peng, S., Ding, Y., Wen, Z., Chen, Y., Cao, Y., and Ren, J.: Spatiotemporal change and trend analysis of potential evapotranspiration over the Loess Plateau of China during 2011 – 2100, Agric. For. Meteorol., 233, 183 – 194, doi:10.1016/j.agrformet.2016.11.129, 2016.

Peng, T., Liu, K., Wang, C., and Chuang, K.: A water isotope approach to assessing moisture recycling in the island-based precipitation of Taiwan: A case study in the western Pacific, Water Resour. Res., 47, doi:10.1029/2010wr009890, 2011.

Phillips, D. L., and Gregg, J. W.: Uncertainty in source partitioning using stable isotopes, Oecologia, 127, 171 – 179, doi:10.1007/s004420000578, 2001.

520 Qin, Y., Lei, H., Yang, D., Gao, B., Wang, Y., Cong, Z., and Fan, W.: Long-term change in the depth of seasonally frozen ground and its ecohydrological impacts in the Qilian Mountains, northeastern Tibetan Plateau, J. Hydrol., 542, 204–221, doi:10.1016/j.jhydrol.2016.09.008, 2016.

Raz-Yaseef, N., Rotenberg, E., and Yakir, D.: Effects of spatial variations in soil evaporation caused by tree shading on water flux partitioning in a semi-arid pine forest, Agric. For. Meteorol., 150, 454–462, doi:10.1016/j.agrformet.2010.01.010,
525 2010.

Sang, L., Zhu, G., Xu, Y., Sun, Z., Zhang, Z., and Tong, H.: Effects of agricultural Large-And Medium-Sized reservoirs on hydrologic processes in the arid Shiyang River basin, northwest China, Water Resour. Res., 59, doi:10.1029/2022wr033519, 2023.

Skrzypek, G., Mydłowski, A., Dogramaci, S., Hedley, P., Gibson, J. J., and Grierson, P. F.: Estimation of evaporative loss
530 based on the stable isotope composition of water using Hydrocalculator, J. Hydrol., 523, 781 – 789, doi:10.1016/j.jhydrol.2015.02.010, 2015.

Stein, A. F., Draxler, R. R., Rolph, G. D., Stunder, B. J. B., Cohen, M. D., and Ngan, F.: NOAA's HYSPLIT Atmospheric Transport and Dispersion Modeling system, Bull. Am. Meteorol. Soc., 96, 2059 – 2077, doi:10.1175/bams-d-14-00110.1, 2015.

535 Sun, X., Wilcox, B. P., and Zou, C. B.: Evapotranspiration partitioning in dryland ecosystems: A global meta-analysis of in situ studies, J. Hydrol., 576, 123–136, doi:10.1016/j.jhydrol.2019.06.022, 2019.

Tague, C. L., Moritz, M., and Hanan, E.: The changing water cycle: The eco-hydrologic impacts of forest density reduction in Mediterranean (seasonally dry) regions, Wiley Interdiscip. Rev. Water, 6, doi:10.1002/wat2.1350, 2019.

Tao, N. S., Zhen-Yu, N. L., Jie, N. Z., Wei, N. H., Yue, N. L., and Gang, N. T.: Spatial distribution and seasonal variation
540 characteristics of global atmospheric moisture recycling, Acta Phys. Sin., 63, 099201, doi:10.7498/aps.63.099201, 2014.

Teo, H. C., Raghavan, S. V., He, X., Zeng, Z., Cheng, Y., Luo, X., et al.: Large-scale reforestation can increase water yield and reduce drought risk for water - insecure regions in the Asia - Pacific, Glob. Change Biol., 28, 6385 – 6403, doi:10.1111/gcb.16404, 2022.

Wang, P., Yamanaka, T., Li, X.-Y., and Wei, Z.: Partitioning evapotranspiration in a temperate grassland ecosystem:
545 Numerical modeling with isotopic tracers, Agric. For. Meteorol., 208, 16–31, doi:10.1016/j.agrformet.2015.04.006, 2015.

Wang, S., Wang, L., Zhang, M., Shi, Y., Hughes, C. E., Crawford, J., et al.: Quantifying moisture recycling of a leeward oasis in arid central Asia using a Bayesian isotopic mixing model, J. Hydrol., 613, 128459, doi:10.1016/j.jhydrol.2022.128459, 2022.

Wang, S., Zhang, M., Che, Y., Chen, F., and Qiang, F.: Contribution of recycled moisture to precipitation in oases of arid
550 central Asia: A stable isotope approach, Water Resour. Res., 52, 3246–3257, doi:10.1002/2015wr018135, 2016.

Wei, Z., Lee, X., Wen, X., and Xiao, W.: Evapotranspiration partitioning for three agro-ecosystems with contrasting moisture conditions: a comparison of an isotope method and a two-source model calculation, Agric. For. Meteorol., 252, 296–310, doi:10.1016/j.agrformet.2018.01.019, 2018.

Wyatt, C. J. W., O'Donnell, F. C., and Springer, A. E.: Semi‑Arid aquifer responses to forest restoration treatments and
555   climate change, Ground Water, 53, 207–216, doi:10.1111/gwat.12184, 2014.

Yang, Y., Chen, R., Song, Y., et al.: Sensitivity of potential evapotranspiration to meteorological factors and their elevational
gradients in the Qilian Mountains, northwestern China, J. Hydrol., 568, 147–159, 2019.

Yao, Y., Liu, S., and Shang, K.: Daily MODIS-based Land Surface Evapotranspiration Dataset of 2019 in Qilian Mountain
Area (ETHi-merge V1.0), National Tibetan Plateau / Third Pole Environment Data Center,
560   doi:10.11888/Meteoro.tpdc.270407, 2020.

Yepez, E. A., Huxman, T. E., Ignace, D. D., English, N. B., Weltzin, J. F., Castellanos, A. E., and Williams, D. G.:
Dynamics of transpiration and evaporation following a moisture pulse in semiarid grassland: A chamber-based isotope
method for partitioning flux components, Agr. Forest Meteorol., 132, 359–376, doi:10.1016/j.agrformet.2005.09.006, 2005.

Zhang, M. and Wei, X.: Deforestation, forestation, and water supply, Science, 371, 990–991, doi:10.1126/science.abe7821,
565   2021.

Zhang, R., Xu, X., Liu, M., Zhang, Y., Xu, C., Yi, R., and Luo, W.: Comparing evapotranspiration characteristics and
environmental controls for three agroforestry ecosystems in a subtropical humid karst area, J. Hydrol., 563, 1042–1050,
doi:10.1016/j.jhydrol.2018.06.051, 2018.

Zhang, Y., Gentine, P., Luo, X., Lian, X., Liu, Y., Zhou, S., et al.: Increasing sensitivity of dryland vegetation greenness to
570   precipitation due to rising atmospheric CO2, Nat. Commun., 13, doi:10.1038/s41467-022-32631-3, 2022.

Zhang, Z., Zhu, G., Pan, H., Sun, Z., Sang, L., and Liu, Y.: Quantifying recycled moisture in precipitation in Qilian
Mountains, Sustainability, 13, 12943, doi:10.3390/su132312943, 2021.

Zhao, C., Zhang, R., Wang, Y.: Cold and Arid Research Network of Lanzhou university (an observation system of
Meteorological elements gradient of Dayekou Station, 2019), National Tibetan Plateau / Third Pole Environment Data
575   Center, doi:10.11888/Meteoro.tpdc.270799, 2020.

Zhao, C., Zhang, R., Wang, Y.: Qilian Mountains integrated observatory network: Cold and Arid Research Network of
Lanzhou University (an observation system of meteorological elements gradient of Dayekou Station, 2018), National
Tibetan Plateau / Third Pole Environment Data Center, doi:10.11888/Geogra.tpdc.270169, 2019.

Zhao, C., Zhang, R., Zhao, C.: Cold and Arid Research Network of Lanzhou university (an observation system of
580   Meteorological elements gradient of Sidalong Station, 2021), National Tibetan Plateau / Third Pole Environment Data
Center, doi:10.11888/Atmos.tpdc.272365, 2022.

Zhao, C., Zhang, R., Zhao, C.: Cold and Arid Research Network of Lanzhou university (an observation system of
Meteorological elements gradient of Sidalong Station, 2020), National Tibetan Plateau / Third Pole Environment Data
Center, doi:10.11888/Meteoro.tpdc.271378, 2021.

585   Zhu, G., Guo, H., Qin, D., Pan, H., Zhang, Y., Jia, W., and Ma, X.: Contribution of recycled moisture to precipitation in the
monsoon marginal zone: Estimate based on stable isotope data, J. Hydrol., 569, 423–435, doi:10.1016/j.jhydrol.2018.12.014,
2018.

Zhu, G., Liu, Y., Shi, P., Jia, W., Zhou, J., Liu, Y., et al.: Stable water isotope monitoring network of different water bodies in Shiyang River basin, a typical arid river in China, Earth Syst. Sci. Data, 14, 3773–3789, doi:10.5194/essd-14-3773-2022, 2022.

Zhu, G., Wang, L., Liu, Y., Bhat, M. A., Qiu, D., Zhao, K., et al.: Snow-melt water: An important water source for Picea crassifolia in Qilian Mountains, J. Hydrol., 613, 128441, doi:10.1016/j.jhydrol.2022.128441, 2022.